Rapid Communications in Mass Spectrometry

WILEY

Rapid Communications in Mass Spectrometry

RESEARCH ARTICLE OPEN ACCESS

A Laser Ablation ICP-MS Protocol for High-Resolution Iodine-to-Calcium Ratio (I/Ca) Analysis on Corals

Ashley N. Prow-Fleischer | Zunli Lu

Department of Earth and Environmental Sciences, Syracuse University, Syracuse, New York, USA

Correspondence: Ashley N. Prow-Fleischer (asprow@syr.edu)

Received: 12 July 2024 | **Revised:** 16 January 2025 | **Accepted:** 23 January 2025

Funding: This work was supported by the Geological Society of America William B. & Dorothy Heroy Research Grant to A.N.P. and the National Science Foundation EAR 2121445 to Z.L.

Keywords: I/Ca | LA-ICP-MS | Laser Ablation | Coral | carbonate standards

ABSTRACT

Rationale: Corals are continuous, time-resolved archives of ambient seawater geochemistry and can extend climate records beyond direct monitoring. The iodine-to-calcium (I/Ca) ratio may be a proxy for local oxygen depletion in corals, but the current solution-based ICP-MS protocol limits sampling resolution. A protocol was developed for rapid analysis of coral I/Ca using laser ablation ICP-MS.

Methods: Two reference materials, a powdered coral (JCp-1) and a synthetic carbonate (MACS-3), were compared for precision in measuring Sr, Mg, I, Ba, and U. Then, the influence of laser parameters (spot size, fluence, repetition rate, and scan speed) on iodine sensitivity from the reference material was evaluated to optimize laser settings for accurate and reproducible I/Ca calibration. Then, I/Ca was measured in line scans along and across the ambulacrum in a *Diploria labyrinthiformis* coral.

Results: We find that JCp-1 has greater precision in measuring iodine, as well as other traces, compared to MACS-3. At a 10 Hz repetition rate, spot sizes from 150 to 85 μm obtained concentrations in agreement with certified values, but higher repetition rates overestimated iodine concentrations from JCp-1. Certain scan speeds and fluence can introduce noise, likely due to matrix effects, but the signal-to-noise ratio can be improved by adjacent-average filtering. Using this simple data filtering routine and optimized laser settings, the highest resolution for accurate I/Ca analysis is < 100 μm. While the fine-scale (< 250 μm) I/Ca variabilities in parallel transects in a coral sample likely resulted from biomineralization processes, large -scale features (> 500 μm) along the ambulacrum tend to correlate.

Conclusions: LA-ICP-MS has great potential for accurate, high-resolution I/Ca profiling in corals using JCp-1 as a calibration standard. Because of compositional variability near centers of calcification, it is important to pay attention to how the laser transect is aligned relative to skeletal elements, which may incorporate iodine differently.

1 | Introduction

Corals are unique archives for resolving climate variability. Several trace element-to-calcium (e.g., Sr, Mg, Ba, and U) ratios are proxies for reconstructing past environmental conditions such as temperature, pH, and salinity [1–3]. It is suggested that the I/Ca in scleractinian (aragonitic) corals may be used for detecting changes in local oxygen saturation [4]. The current protocol for measuring I/Ca in skeletal material using solution-based ICP-MS, adapted for foraminiferal tests and bulk carbonate, maintains long-term reproducibility using the external standard JCp-1, a powdered aragonitic *Porites* sp. coral [5, 6]. However, the solution-based protocol, which involves micro-milling of bulk carbonate, does not

allow high-resolution studies on corals. We aim to develop a protocol for in situ I/Ca measurements using laser ablation ICP-MS.

Previous attempts to measure iodine in corals using microbeam techniques reported that low signal-to-noise ratios due to high backgrounds and a lack of suitable matrix-matched standards were significant challenges [7, 8]. The only carbonate-based laser ablation standard commercially available with certified iodine concentration is the United States Geological Survey (USGS) MACS-3 [9], but it is frequently reported as having a heterogeneous distribution of not only iodine but other useful tracers [10, 11]. Pelletized JCp-1 has been used as a reference material for the calibration of elemental/Ca ratios in corals using laser ablation and was found to have a uniform distribution of several elements, including Sr, Ba, Mg, and U, but the spatial distribution of I has not been tested [12, 13].

To develop a laser ablation protocol for iodine analysis in carbonate matrices, we first compare the reproducibility and homogeneity of iodine distribution in MACS-3 and JCp-1. Then, we explore the effects of laser settings on several parameters (spot size, fluence, scan speed, and repetition rate) on iodine sensitivity and precision measurements from JCp-1 to establish a range of ideal laser operating conditions. Last, using the optimized laser settings, we measure I/Ca along and across the ambulacrum from a cross-section of a *Diploria labyrinthiformis* coral.

2 | Experimental

2.1 | Sample Preparation

About 2 g of powdered JCp-1 from the Japan Geological Survey was pelletized without binders in a 13-mm evacuable press and mounted on a glass slide [6]. A pressed powder MACS-3 pellet was obtained from the USGS in 2013 before it was discontinued [14]. A puck ~10 cm in diameter was cut transversely from a core of *D. labyrinthiformis,* taken from near Bermuda at shallow (< 50 m) depths. The coral was polished with 30-, 12-, 9-, and 3-μm grit paper and sonicated in 0.1% H_2O_2 to remove organic contaminants.

2.2 | Analytical Methods

All data were line scans collected on a ThermoScientific iCap-TQ mass spectrometer at the State University of New York School of Environment Science and Forestry (SUNY-ESF) running in standard mode (Table 1). The materials were ablated using a Teledyne Analyte Excite 193 nm ArF excimer laser (Table 1). The tuning routine involved line scanning the glass standard NIST 612 to minimize oxide ($ThO^+/Th < 0.3$) and doubly charged ion ($^{137}Ba^{++}/^{137}Ba$) formation and maximize sensitivity (^{59}Co, ^{115}In, and $^{238}U > 10\,000$ counts per second [cps]). Ablations were carried out in a pure He atmosphere. The analyte was carried in He and then mixed with argon via a "Y" connector before entering the plasma. Plasma power was set to high output (1.5 kW) with high gas throughput (8.0 L·min^{-1}) to mitigate transport effects due to the complex and high-proportion matrix.

To maximize counting times for each element, only a few isotopes that are common coral geochemical tracers were monitored: ^{25}Mg, ^{43}Ca, ^{44}Ca, ^{88}Sr, ^{127}I, ^{138}Ba, and ^{238}U. ^{43}Ca was used as an internal standard for all monitored isotopes to correct for sensitivity drift within single-line scans and element/Ca ratios were taken relative to ^{44}Ca. Because ^{127}I has low ionization efficiency and high backgrounds, its dwell time was set to 0.4 s to provide better counting statistics [11]. The dwell times of all other monitored elements were set to 0.1 s.

For the reference materials, lines were scanned for ~250 s starting with the laser on with a 30-s background acquisition. Because after the laser is turned on, there was an ~25-s time frame where the signal decays before stabilizing (Figure S1), an evaluation window is defined as the 200 s after the signal baseline becomes stable. The signal within the evaluation window was used to calculate precision metrics and for calibration of the coral sample. Instrument stability was ensured over long analytical sessions (> 6 h) by online monitoring of the reference material signal-to-background intensity ratio of ^{127}I and the element-to-^{43}Ca of all elements. Two scans of the reference material using an 85-μm spot size were performed every 30 min to assess long-term behavior. A signal-to-background ratio > 2.0 for ^{127}I was considered acceptable.

Data reduction and quantitation of figures of merit were performed offline in Origin (Pro) (Version 2024) [15] following the methods of Longerich (1996) [16] and Sinclair et al. (1998) [17]. For every acquisition, 30 s of background signal was collected with the shutter open and laser off (Table 1). Background subtraction was performed using the PeakAnalyzer function in Origin to automate the process, but the principle is the same as subtracting the average background signal from every point along the entire acquisition. This method is justified because there is little sensitivity drift within a single-line scan, and so the baseline does not need to be corrected (Figure S1). The background-subtracted signal of all elements was then normalized to ^{43}Ca.

A 50% adjacent-averaging filter with a 15-point moving window was applied to the normalized signal intensity in the time domain to smooth outlying points and reduce noise (Figure S2) [18]. This filter averages points continuously along the line scan and excludes any values greater or less than 50% of the adjacent average of the current point, *i*. For a 15-point window, every ~7.5 points before and after point *i* are averaged into a new point, then continuing to point *i* + *1,* thus maintaining the same number of points. This filter and window size were used because they removed single-point outliers at the sweep times (1.8 s) employed without diminishing data quality (Figure S2). While there are other filtering algorithms, adjacent averaging is ideal for reducing noise while retaining sharp step changes in signal (e.g., from background to laser on); it is simple enough for routine analysis in spreadsheets and is satisfactory for trace element ratios in corals [13, 17].

Repeatability (same-day precision) and reproducibility (different-day precision) in measuring ^{25}Mg, ^{88}Sr, ^{127}I, ^{138}Ba, and ^{238}U were calculated for JCp-1 and MACS-3. Measurements for determining precision metrics used the same laser parameters (Table 1). Precision is reported as the relative standard deviation (RSD, %) of the filtered evaluation window signal averaged from three replicate scans. Following Sinclair (1998) [17], the heterogeneity of the reference materials is calculated from one scan as

TABLE 1 | Instrument specification and operating conditions.

ICP-MS	ThermoScientific iCap-TQ
Tuning (NIST 612)	$^{232}ThO^{+}/^{232}Th < 0.03$ (oxides) ^{115}In (cps), ^{238}U, and $^{59}Co > 10\,000$ (sensitivity) $^{137}Ba^{++}/^{137}Ba < 0.3$ (doubly charged ions)
Acquisition mode	Pulse counting
Acquisition time (reference materials)	30-s background (shutter open/laser off) + 250-s laser transect + 20-s washout time (laser off)
Acquisition time (coral)	Preablation + 30-s background (shutter closed/laser off) + up to 15-min continuous ablation + 60-s washout
Cycle time	1.8 s
Dwell time for isotopes monitored	0.1 s: ^{25}Mg, ^{43}Ca, ^{44}Ca, ^{88}Sr, ^{138}Ba, and ^{238}U 0.4 s: ^{127}I Total sweep time: 1.8 s
Laser system	Telydyne Analyte Excite 193 nm ArF Excimer
Laser mode	Standard mode (no reaction gas)
Nebulizer gas	~0.916 L/min Ar
Auxiliary gas	~0.800 L/min Ar
Carrier gas flow	~0.8 L/min He (MFC1: 0.5 L/min; MFC2: 0.3 L/min)
Plasma power	1550 W

Laser settings	**Tuning**	**Reference material experiments**	**Coral experiments**
Fluence (energy density; J·cm^{-2})	2.13	1.5, 2.0, and 2.5	2.0
Repetition rate (Hz)	10	5, 10, and 20	10
Spot size (μm, circle)	110	50, 85, and 150	85
Scan speed (μm·s^{-1})	2	1, 3, and 5	3

$$\%heterogenity = \frac{Maximum\ intenstiy\ (cps) - Miniumum\ intensity\ (cps)}{average\ intenstiy\ (cps)} \times 100\% \quad (1)$$

using background subtracted but not filtered intensities of the evaluation window. Limits of detection (LOD) for ^{127}I from JCp-1, using MACS-3 as a calibration standard, were calculated using Poisson counting statistics [19].

Line scans of the coral were preablated to remove surface contaminants and ran for no longer than 15 min to limit sensitivity drift within a single scan. The background-subtracted and normalized intensity (cps) signals from the coral scans were converted to concentrations using methods outlined in Longerich (1996) and ratioed with the ^{44}Ca concentrations accounting for isotope abundance. Filtering was applied to the elemental ratios.

2.3 | Experiments to Evaluate the Precision of Carbonate Standards

A series of experiments were performed to determine both the best reference material and the optimized laser parameters for measuring the monitored element/Ca ratios, especially I/Ca, in the coral. First, three replicate line scans were taken on both JCp-1 and MACS-3. The average reproducibility, repeatability, and heterogeneity of each element were calculated.

2.3.1 | Experiments to Determine Optimal Laser Settings

Reference material comparison experiments were performed at the same laser settings of 85-μm circular spot size, 10-Hz repetition rate, 3-μm·s^{-1} scan speed, and 2-J·cm^{-2} fluence. Next, to optimize each laser setting for the highest sensitivity and precision of I/Ca analyses, four parameters were tested at three settings: spot size (53, 85, and 150 μm), repetition rate (5, 10, and 20 Hz), scan speed (1, 3, and 5 μm s^{-1}), and fluence (1.5, 2.0, and 2.5 J·cm^{-2}). The setting of each parameter was systematically changed while keeping the other settings at their intermediate value for a total of 12 combinations. Because repetition rate and spot size are the two laser parameters that increase the volume of ablated material introduced into the mass analyzer [20], the combined effects of these two settings on the accuracy of iodine determination from JCp-1, using MACS-3 for external calibration, were assessed. Spot size was decreased from 150 to 50 μm at 10- and 20-Hz repetition rates, and the iodine concentration and LOD were calculated. The

combination of spot size and repetition rate where the calculated concentration's uncertainty overlaps with the certified value ($5.5 \pm 0.2\,\mu g/g$) [6] is considered a suitable setting combination for analyses on corals. Here, concentration uncertainty is defined as the average standard deviation of the evaluation window signal from two replicate scans.

2.3.2 | Experiments to Measure I/Ca in Coral

Last, the reference material and laser settings that gave the most accurate and precise iodine concentrations were used to measure element/Ca from scans along and across the ambulacral groove of *D. labyrinthiformis*. To prevent the likelihood of iodine baseline drift, scans were kept to less than 15 min and bracketed by both JCp-1 as the external standard. Because switching from the harder coral skeleton to the softer reference material sometimes introduced decaying sensitivity in the first part of the scan, the acquisition of reference material was performed twice, and the best was used for analyses.

3 | Results and Discussion

3.1 | Long-Term Instrument Stability

Sensitivity is expected to drop for various reasons throughout long analytical sessions. Because glass standards used for tuning (e.g., NIST 612) do not have detectable iodine, it was most instructive to assess long-term instrument behavior by monitoring the consistency of elemental/^{43}Ca and signal-to-background ratios from the carbonate standards (Figure S3). Sessions were generally kept to less than 6 h before retuning due to some drift in iodine sensitivity over time, determined by a slight reduction in ^{127}I/^{43}Ca and coincident increase in ^{127}I signal-to-background ratios. We recommend maintaining fluctuations in ^{127}I/^{43}Ca to less than 10% to ensure calibration accuracy.

3.2 | Comparison of Carbonate Standards Precision Metrics

The homogeneity of elemental composition in reference materials directly influences the accuracy and repeatability of analyses. Metrics of precision and matrix heterogeneity for MACS-3 and JCp-1 were compared for five elements (Mg, Sr, I, Ba, and U; Table 2). Unfiltered ^{127}I signals from a single scan of MACS-3 have a greater compositional range (heterogeneity) compared to JCp-1 (Figure 1; Table 2). Repeatability and reproducibility were calculated on filtered signals. JCp-1 had better repeatability for ^{25}Mg (7.35% vs. 15.1%), ^{88}Sr (4.51% vs. 12.5%), ^{127}I (9.6% vs. 31.3%), and ^{238}U (6.33% vs. 20.2%), whereas MACS-3 had better precision only for ^{138}Ba (16.7% vs. 33.0%). Likewise, JCp-1 had better reproducibility over three analytical sessions for ^{25}Mg (9.6% vs. 23.5%) and ^{88}Sr (10.5% vs. 18.5%) and was considerably better for ^{127}I (7.8% vs. 44.2%) and ^{238}U (9.1% vs. 46.7%), but MACS-3 had slightly better but still low reproducibility for ^{138}Ba (28.6% vs. 52.2%). JCp-1 also displayed lower heterogeneity for all monitored elements, especially for ^{127}I (1.03% vs. 30.0%).

The repeatability of ^{127}I from JCp-1 using solution-based ICP-MS is generally < 1% [22]. There are no comparable laser ablation studies that examine ^{127}I from carbonate standards but we have similar precision (< 10%) reported by Caulfield et al. (2020) [23] in their comparison of ^{127}I ablated from glass standards who regard precisions of < 10% RSD as excellent considering the high ionization potential of halogens.

JCp-1 had a lower background signal for all elements except for ^{127}I with higher backgrounds (> 11 000 cps) compared to MACS (> 8500 cps) while also varying between sessions and over the duration of one session. This is an important consideration because high backgrounds can affect the limits of detection and accuracy. Different ^{127}I backgrounds between standards have also been reported by Kendrick et al. (2020) [24] in their analysis of iodine from silicate glasses. Iodine has few gas-based polyatomic interferences that could arise from the He-based plasma that cannot be minimized by tuning [25, 26]. Instead, Kendrick et al. (2020) attributed elevated backgrounds between sessions to contamination in the ICP-MS interface due to insufficient transport from previous runs. This was partly mediated during a session by having long washout times. In JCp-1, signal-to-background ratios of ^{127}I steadily rise over the duration of a session (from 2.1 to 2.7, Figure S3) as the background signal decreases over time, possibly due to flushing at the high gas flow rates. In the experiment where two sequential scans of the reference material were taken every 30 min, the second scan almost always had a lower signal-to-background ratio due to higher background, but the RSD during acquisition were comparable. This is the reason for adding a 60-s washout between runs with coral samples, which reduced the variability in background.

For the other monitored elements, Lazartigues et al. (2014) [27] similarly reported high heterogeneity and low precisions (ranging from 46% to 94% RSD) for ^{25}Mg, ^{88}Sr, ^{43}Ca, and ^{138}Ba in MACS-3 using spot sizes of 5 μm and suggested that high heterogeneity was related to the small spot size. Jochum et al. (2014) [28] also observed spot size-dependent precision in MACS-3 from spot sizes ranging from 10 to 55 μm. It was proposed that high variability in MACS-3 was due to fractionation processes whereby fragments with different sizes become ablated from the pellet leading to compositional variability during vaporization. This concept is supported by Hathorne et al. (2008) [12], who performed a particle trap study in the ablation cell to compare fractionation between JCp-1 and an in-house synthetic carbonate standard. They found that the shapes and size distributions of ablated particles were related to both laser settings and the material, and that JCp-1 had a relatively homogenous ablation particle size with compositions comparable to the bulk values. The synthetic carbonate standard had microsize particles of irregular and angular shape in a mesh of smaller particles, leading to differences between bulk and particle composition in some elements. This was attributed to photomechanical fracturing and ejection along the lines of weakness in the calcite grains. Increasing fluence from 4 to 10 $J \cdot cm^{-2}$ also increased the proportion of irregularly shaped particles [12].

MACS-3 was powdered by dry milling, which in synthetic carbonate standards creates a range of grain sizes no smaller than 5 μm [29]. Boer et al. (2022) [14] used a nano milling technique

TABLE 2 | Comparison of MACS-3 and JCp-1 standards.

		Reported concentration (μg/g)[a]	Average background (cps) ($n=5$)	Average (cps) ($n=5$)[b]	Standard deviation ($n=5$)[c]	Repeatability (relative standard deviation RSD%) ($n=5$)[d]	Heterogeneity (%) ($n=1$)[e]	Reproducibility ($n=3$)[f]
^{25}Mg	MACS-3	1880 ± 300	74.88	633 218.9	168.3	15.1	19.6	23.5
	JCp-1	972 ± 8	**50.00**	415 029.9	**80.1**	**7.35**	**5.09**	**9.6**
^{88}Sr	MACS-3	6640 ± 200	853	55 682 798.4	**454.0**	12.5	53.56	18.5
	JCp-1	7240 ± 40	**71.22**	71 353 841.3	583.9	**4.51**	**22.3**	**10.5**
^{127}I	MACS-3	20	**8655.2**	90 812.06	6.0	31.3	30.0	44.2
	JCp-1	5.5 ± 0.2	11 678	27 314.84	**0.72**	**9.6**	**1.03**	**7.8**
^{138}Ba	MACS-3	58.7 ± 2	10.0	575 279	6.59	**16.7**	**18.9**	**28.6**
	JCp-1	6.97 ± 0.59	**0.55**	109 499	**1.00**	33.0	84.0	52.2
^{238}U	MACS-3	1.41 ± 0.07	0.41	17 916.85	**0.27**	20.2	1.5	46.7
	JCp-1	2.67 ± 0.12	**0.33**	34 682.04	1.03	**6.33**	**1.1**	**9.1**

Note: Comparison of precision metrics of MACS-3 and JCp-1 from sequential replicate analyses of 250-s scans at the following laser settings: 85-μm spot size, 3-μm·s^{-1} scan speed, 2-J·cm^{-2} fluence, and 10-Hz repetition rate. For all precision metrics (standard deviation, reproducibility, and repeatability) line scans were background-subtracted by subtracting the background (cps) from the raw average (cps). All but heterogeneity were filtered using 50% adjacent averaging. For each element, the bolded value indicates the better value.

[a]Concentrations retrieved from GeoRem database [21]. Reported values were obtained using 193-nm LA-ICP-MS where available. All others are from solution-ICP-MS (Mg, Sr, and I for JCp-1). Here, the word "reported" is used to distinguish it from published "certified" values. Uncertainties are ±2σ.

[b]The raw (e.g., not background-subtracted) average signal intensity (cps) of 5 replicate line scans over the 200-s evaluation window (the most stable area of acquisition). Here, raw averages are provided so signal-to-background ratio can be compared.

[c]Reported as the standard deviation of the 200-s evaluation window's filtered signal averaged over 5 replicate line scans.

[d]Repeatability (same-day precision) is reported as relative standard deviation (RSD, %) and calculated as the standard deviation of the evaluation window divided by the average signal intensity averaged over 5 replicate line scans.

[e]Heterogeneity is calculated from one scan as [maximum intensity (cps) − minimum intensity (cps)]/average (cps) * 100%, of the background-subtracted, but not filtered, evaluation window signal.

[f]Reproducibility (different-day precision) is calculated as the average RSD from three scans taken ~2 months apart (December 2023, February 2024, and April 2024).

on MACS-3 and JCp-1, which produces particles < 250 nm, and obtained comparable RSDs between the standards for several elements. This suggests that the heterogeneity of MACS-3 derives partly from large grain size distribution. Although we used larger spot sizes for these experiments (85 μm), more refractory elements (e.g., high ionization potential) become easier to vaporize with a small, consistent ablated particle size [12, 30]. The lower heterogeneity of JCp-1, even at larger spot sizes compared to these other studies, suggests that its photomechanical response to the laser is more consistent than MACS-3 and would produce more reproducible signals using the same laser settings.

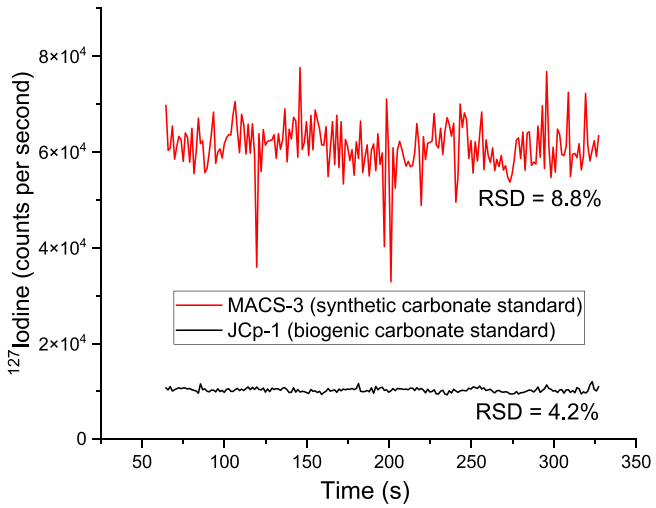

FIGURE 1 | Variation of raw, unfiltered iodine signal from the evaluation window of a single scan on MACS-3 (red) and JCp-1 (black).

Together, the higher precision and greater homogeneity of not only ^{127}I but also Sr, Mg, and U, make JCp-1 a more suitable standard compared to MACS-3 for external calibration of carbonate matrices. The remainder of the experiments used JCp-1 to test the effects of laser settings on the ^{127}I signal and for calibration against the corals.

3.3 | Effect of Laser Settings on Precision

A series of tests were performed that systematically changed one laser setting while keeping the others at intermediate settings (Table 1) to determine the optimal parameterizations for the most repeatable and accurate iodine signal from JCp-1. We compare both unfiltered and filtered background-subtracted ^{127}I signals for 12 total scans (Figure 2) to assess the influence of both the laser setting and the filter on repeatability. Compared to the scan using all intermediate settings, which had an unfiltered RSD of 5.87% for ^{127}I, all combinations of settings resulted in higher RSD except for a spot size of 50 μm by a small margin (5.67%). A fluence of 2.5 J·cm^{-2} and a scan speed of 1 μm·s^{-1} had the lowest repeatability of 69.0% and 53.6%, respectively (Figure 2b), followed by a scan speed of 5 μm·s^{-1} (28.6%). The decrease in precision at higher fluence may be due to uneven size distribution of ablation particles, especially from the relatively soft matrix [12, 24]. While increasing scan speed (from 3 to 5 μm·s^{-1}) can result in inefficient transfer, resulting in a "blurred" signal and reduced sensitivity, lowered scan speed (3 to 1 μm·s^{-1}) may also contribute to more thermal degradation and lowered precision because the laser is focused on one area for longer duration [31, 32]. This is important considering the volatility of iodine, which may be lost from thermal degradation.

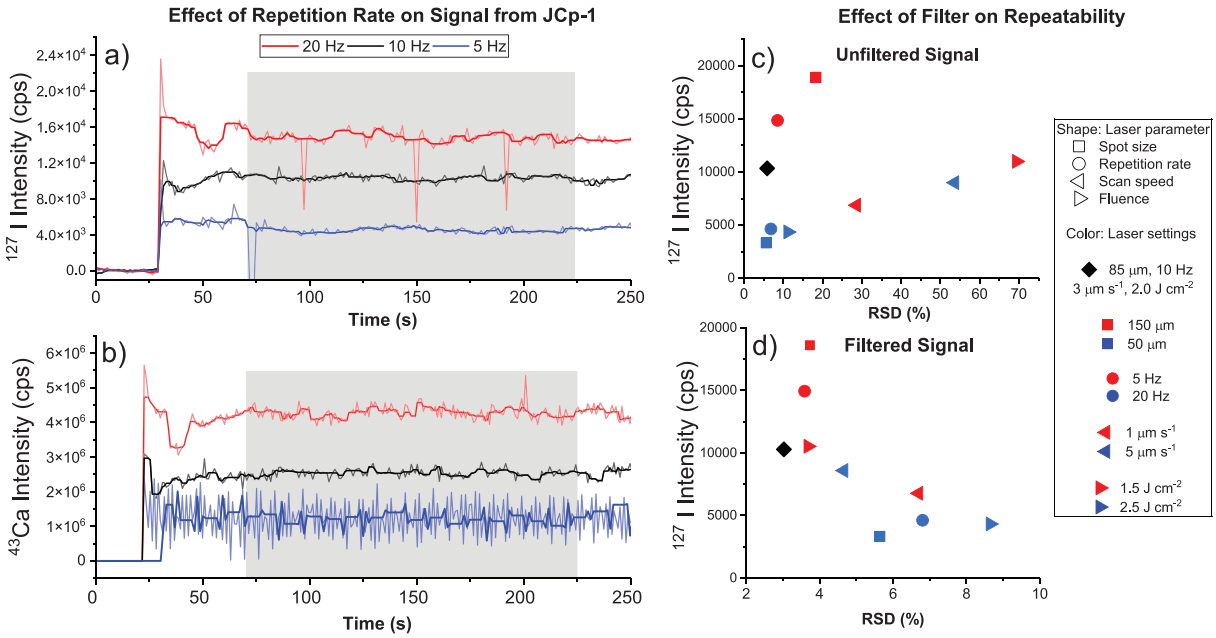

FIGURE 2 | (a) background-subtracted unfiltered (faint lines) and filtered (dark lines) iodine signal using 10-Hz (black), 20-Hz (red), and 5-Hz (blue) repetition rates (all other settings 85 μm, 2.0 J·cm^{-2}, and 3 μm·s^{-1}). The gray section is the evaluation window used for precision calculations in Panels (c) and (d). (b) Influence of repetition rate on internal standard ^{43}Ca signal. (c) Influence of laser parameters (spot size = square, repetition rate = circle, scan speed = left triangle, and fluence = right triangle) and settings (red and blue) on unfiltered, nonnormalized iodine signal versus precision (RSD) compared to the scan using all intermediate settings (black diamond). (d) The influence of filtering the data in Panel (c).

The adjacent-average filtering improved all precisions to below 9% RSD, with the lowest being, the all-intermediate settings scan down to 3.2% RSD. The 2.5-J·cm^{-2} fluence and 1-μm·s^{-1} scan speed precisions were improved the most by filtering to 3.6% and 4.6%. This simple filtering method effectively removed outliers, which were the main contributors to iodine signal variability. While more computationally involved frequency filtering methods exist, several studies suggest that these methods impose time and computational constraints for routine analyses while not significantly improving signal-to-noise ratio compared to adjacent-averaging [13, 17].

The settings affected the least by filtering were 5-Hz repetition rate and 50-μm spot size with less than 0.05% change in RSD. Spot size likely has little influence on RSD, considering the homogeneity of iodine in the JCp-1 pellet. The time series of the unfiltered iodine signal at a 20-Hz repetition rate shows irregular extreme negative outliers (Figure 2a), which caused slightly higher iodine RSD (8.5%) compared to the 10-Hz (5.8%) and 5-Hz (6.8%) scans, but these outliers were mostly filtered out. Whereas repetition rate had comparatively little influence on iodine variability, at 5 Hz it introduced considerable noise to the internal standard ^{43}Ca signal (Figure 2b) and, therefore, could lead to large uncertainties of calculated ratios. Fehrenbacher et al. (2015) [33] show that in foraminiferal depth profiling, repetition rates lower than 4 Hz resulted in high noise for major elements like ^{43}Ca, whereas the rapid ablation at high repetition rates (> 5 Hz) and high energy density (> 3 J·cm^{-2}) improved signal-to-noise but reduced spatial resolution. The nonuniform sampling of soft materials like JCp-1 at low repetition rates introduces large matrix effects. The results of this study suggest that higher repetition rates can be used (10 Hz) if they are balanced by lower fluence (2 J·cm^{-2}).

A spot size of 150 μm followed by a 20-Hz repetition rate are the only settings that increased iodine sensitivity relative to the scan using all intermediate settings without contributing to greater uncertainty (Figure 2c,d). Larger spot sizes, higher repetition rates, and higher fluence may increase signal simply by increasing the volume of ablated material introduced into the mass analyzer, but photomechanical-driven ablation can result in preferential enrichment or depletion of certain elements in the ejecta plume [34]. For this reason, it is also important to test how spot size and repetition rate may influence the accuracy of measuring iodine from JCp-1.

3.4 | Effects of Spot Size and Repetition Rate on Accuracy

We examined the combined effects of spot size and repetition rate on the accuracy of iodine determination from JCp-1 by decreasing spot size from 150 to 50 μm at 10 and 20 Hz. (Figure 3). At 10 Hz, spot sizes from 150 to 85 μm obtained concentrations in agreement (here defined as having overlapping error bars) with the certified value (5.5 ± 0.2 μmol/mol) [6], but only the 85 μm size agreed at 20 Hz. The LOD at 10 Hz ranged from 0.25 μg/g at 150 μm up to 2.8 μg/g at 50 μm and at 20 Hz ranged from 0.14 μg/g at 150 μm to 1.95 μg/g at 50 μm. The lowest LOD for 10 Hz was obtained at 110 μm (0.18 μg/g) and for 20 Hz at 85 μm (0.13 μg/g). At 50 μm, the raw acquisition

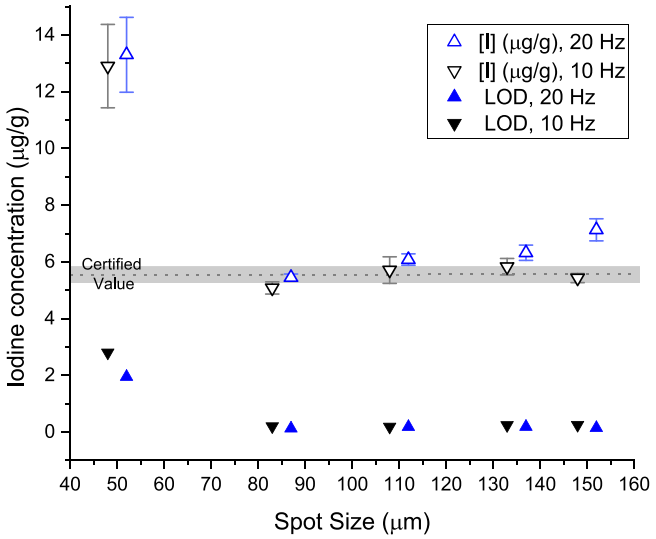

FIGURE 3 | Variability in iodine concentration (open symbols) and limit of detection (closed) measured from JCp-1 at different spot sizes and 10-Hz (down triangle) and 20-Hz (up triangle) repetition rates. The certified value 5.5 ± 0.2 μg/g is represented by the dashed line and gray error bar [6]. MACS-3 was used for external calibration.

signal was too low to distinguish from the background, leading to very high LOD and artificially high sensitivity. Thus, the smallest spot size that can be used to produce an accurate signal from JCp-1 is 85 μm at 10 or 20 Hz. Higher (20 Hz) repetition rates have lower LOD but produce less accurate signals.

To calculate the sampling resolution achievable for coral analyses at an 85-μm spot size, we consider that features of the adjacent-average filter less than half the size of the moving window are removed while keeping the same number of points. At a 3-μm·s^{-1} scan speed and sweep time of 1.8 s (Table 1), a point is taken every ~5 μm. Therefore, with a 15-point average, the spatial resolution is 75 μm. Warter and Müller (2017) [35] found that by using slow scan speed (1.5 μm·s^{-1}) and short sweep time (350 ms) with 5-point averaging, a spatial resolution of 4 μm for Sr/Ca can be achieved for continuous profiling in giant clams. While lowering scan speed was shown to reduce precision (Figure 2c), likely by thermal degradation, the filter removed much of the noise (Figure 2d). Thus, reducing scan speed is a reasonable approach to further increase spatial resolution. Also, fewer elements could be monitored to reduce sweep time. Ultimately, due to the low sensitivity of iodine, a large spot size is required, imposing the greatest methodology-based limitation on resolution.

To obtain the highest spatial resolution for coral sampling, we used the smallest spot size that gave accurate values from JCp-1, 85 μm, which required a repetition rate of 10 Hz. At this repetition rate, a fluence of 2.0 J·cm^{-2} is recommended to reduce matrix-related effects. Because there is a compromise to be made between resolution and precision, we chose a scan speed of 3 μm·s^{-1} so we could run longer line scans, which we limited to 15 min to avoid baseline shifts, without having to recalibrate. This combination of scan speed and spot size gives a spatial resolution of < 100 μm depending on the number of points averaged during the signal filtering.

3.5 | I/Ca Profiling in Coral

Features of the skeletal architecture (e.g., density and proximity to living tissues) of corals can influence the distribution of element/Ca ratios and affect proxy interpretation [7, 36]. To test the protocol, we examine the I/Ca distributions along and across the ambulacral groove, which is the convex wall dividing two adjacent corallites that bear the living tissue of *D. labyrinthiformis* (Figure 4) [36]. Because we are interested in spatial distributions rather than temporal, the coral was cut as a cross-section, so we sampled the part of the ambulacrum that was calcified during a single season of growth rather than down its growth axis. Regardless, areas of higher and lower density along the ambulacrum, light appearing darker and lighter under reflected light, respectively, may contribute to signal variability (Figure 5). These light–dark couplets are septa (radiating vertical plates that support the individual corallite), which appear lighter under reflected light and intersect the darker thecal wall of the ambulacrum.

Along the ambulacrum, the parallel line scans 1 and 2, taken 100 μm apart, were about 6000 μm in length and traversed 5 light–dark couplets (Figures 4a and 5). The dark bands average 850 μm in length, and the light bands average 350 μm (Figure 5b). Line scans 3 and 4 are separated by ~450 μm and run across the ambulacrum in opposite directions, and each traverses one light–dark couplet along their path (Figure S5). These scans reveal systematic and significant spatial variabilities in I/Ca. The I/Ca of scan 2, closer to the middle of the ambulacrum, is consistently ~2 μmol/mol lower than scan 1 (Figure 5). The fluctuations in I/Ca recorded in scans 1 and 2 correlate with the light–dark bands in general, possibly reflecting differences in iodine incorporation into these skeletal elements. The range of values across each 6000-μm scan is 2.75 μmol/mol but scan 2 has slightly lower variability ($\sigma = 0.39$) than scan 1 ($\sigma = 0.53$). These features are also observed in other element/Ca ratios, such as Sr/Ca (FigureS5). Scans 3 and 4 show higher concentrations towards the corallites, nearly doubling the I/Ca values found closer to the center of the ambulacrum (Figure 6).

Sun et al. (2023) [4] measured I/Ca using solution-based ICP-MS in several taxa of scleractinian corals living near active dissolved O_2 monitoring stations by micro-drilling along the thecal wall. These corals fell into two statistically separated groups where those occupying areas of dissolved $O_2 > 160$ μmol/kg had average I/Ca values of 9.30 ± 1.75 μmol/mol and where O_2 was < 160 μmol/kg had average I/Ca of 7.53 ± 1.02 μmol/mol. This suggests that I/Ca less than 7.5 μmol/mol could indicate hypoxic conditions during biocalcification. Based on this threshold identified by Sun et al. (2023), the I/Ca of scans 1 and 2, with ranges spanning 5.1 to 7.6 μmol/mol and 3.4 to 5.3 μmol/mol, respectively, could be interpreted to have experienced oxygen depletion. However, the observed spatial variabilities up to 2.75 μmol/mol in I/Ca, even just 100 μm apart in the thecal wall, call for careful microdrilling of coral for solution-based studies. If line scan 1 was taken another 100 μm closer to the corallite, then it is likely that the signal would have been above the hypoxia threshold (Figure 6). This result indicates that further method development and calibration work are required to reveal the true controls of I/Ca signal in corals, especially for application to paleo-records.

The incorporation of trace elements into coral skeletons has been shown to be controlled by both environmental factors and vital effects that control calcification [38, 39]. In deep-sea black corals, high concentrations of iodine and other trace biophilic elements (e.g., Pb, Mn, and Cd) have been reported in "gluing zones" (organic-rich growth layers) between successive growth bands where rapid biocalcification occurs [7, 8]. While *D. labyrinthiformis* does not have gluing zones, transmembrane proteins secreted by soft-bodied tissue that facilitate biomineralization could contribute to the high iodine content near corallites [40]. Furthermore, Cohen et al. (2004) [36] showed that growth rates across the ambulacral groove are faster near the outside edges. Due to how the coral was cut in cross-section, faster extension rates near the edges of the ambulacrum means different growth layers were likely sectioned through, thus contributing to the I/Ca offset in lines 1 and 2 in addition to the curved profile from edge to edge in lines 3 and 4 (Figures 5 and 6). The detailed mechanisms

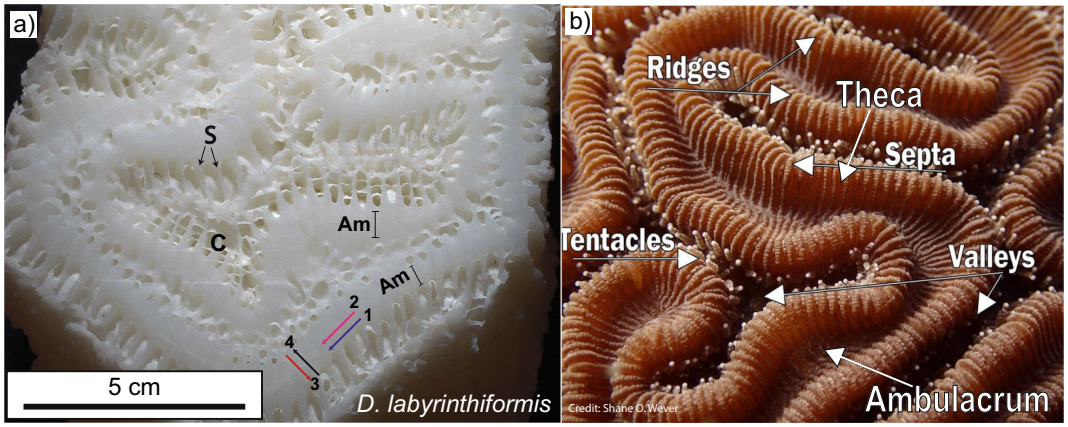

FIGURE 4 | (a) Skeletal architecture of sampled *Diploria labyrinthiformis* cross-section and sampling locations. Soft tissue occupies the corallum (C) arranged in a series of dark thecae (T) and light septae (S) elements that span the ambulacrum (Am). (b) Close-up of living specimen showing same structure in Panel (a) for comparison. Photo taken and replicated with permission by Shane O. Wever at *Coral Reef Restoration Assessment and Monitoring (CRRAM) Laboratory* Nova Southeastern University [37].

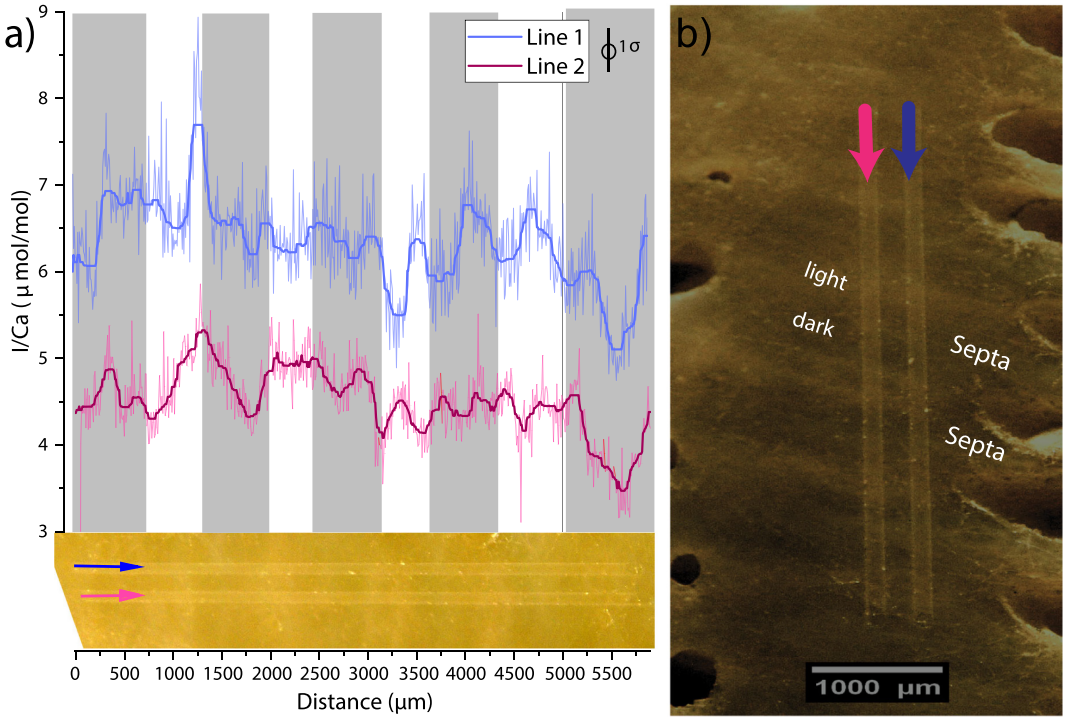

FIGURE 5 | (a) Variation in I/Ca along two line scans on coral. Faint lines are background-subtracted signals with no filtering, and darker lines have a 15-point adjacent average filter applied. The error bar is the standard deviation of JCp-1 evaluation window (±0.5µmol/mol). Gray bands align with dark bands (higher density thecal elements). Line 2 (pink) is translated (~50 µm) horizontally to line up with banding. (b) Close-up of lines 1 and 2 with enhanced contrast to show density-banding of theca and septa. Scale bar 1000 µm.

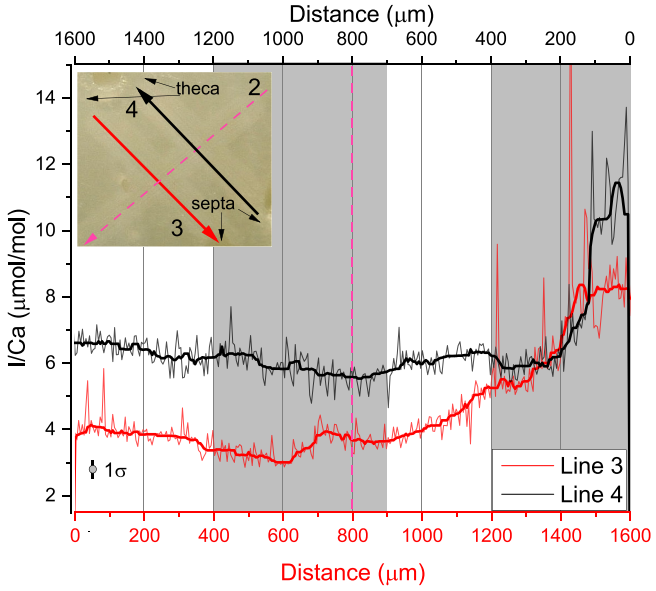

FIGURE 6 | I/Ca variation in scans across the ambulacrum (between adjacent corallites). Insert shows the direction of scans in Figure 5. Gray band indicates high-density areas. The vertical dashed line is the location line 2 would be if it continued through.

driving these I/Ca variabilities across small areas will need to be addressed in future studies.

Despite the estimated resolution of down to 75 µm using the optimized laser settings, the natural resolution of coral records is limited by biocalcification processes [36]. Over the period of a few weeks, the porosity of newly accreted skeleton is gradually filled in such that proxies for age control, like Sr/Ca, can only resolve biweekly signals at the shortest time scales [1, 17, 36]. Although we did not ablate down the growth axis for a temporal signal, it is worth considering for future studies that the average annual growth rates of *D. labyrinthiformis* are $3.0 \pm 0.5\,\text{mm}\cdot\text{yr}^{-1}$ [36]. With an estimated average monthly accretion rate of 200 to 300 µm, using an 85-µm spot size and 3-$\mu\text{m}\cdot\text{s}^{-1}$ scan speed, a biweekly to monthly signal could be resolved with good precision and accuracy if using repetition rates between 10 and 20 Hz.

4 | Conclusions

This study explored the details of external calibration and laser setting optimization for rapid, high-resolution I/Ca sampling in corals by laser ablation ICP-MS. Compared to synthetic carbonate reference material MACS-3, the biogenic aragonitic coral standard JCp-1 is more homogenous and has less matrix-related effects on iodine analysis. When using a soft reference material like JCp-1, to maintain uniform ablation without reducing sensitivity, it is recommended to use a repetition rate between 10 and 20 Hz, a scan speed of $3\,\mu\text{m}\cdot\text{s}^{-1}$, and a fluence of $2.0\,\text{J}\cdot\text{cm}^{-2}$. At these conditions, the smallest spot size that gave accurate iodine estimates from JCp-1 was 85 µm. Using a simple 50% adjacent-averaging filtering routine, a resolution < 100 µm can be achieved for I/Ca at this spot size. This resolution can represent biweekly to monthly growth for some species of coral. In the sampled *D. labyrinthiformis* coral, I/Ca varies across structural features with different densities,

but signals show large-scale similarities over length scales of 500 to 1000 μm. Iodine may accumulate or be highly variable in areas of rapid calcification, such as near soft body tissue, and faster extension rates near these areas may lead to higher signal variability that could obscure proxy interpretations. Because of the compositional variability along different skeletal elements, we recommend sampling down the center of the ambulacrum, where we observed the most stable signals.

Author Contributions

Ashley N. Prow-Fleischer: funding acquisition, conceptualization, investigation, writing – original draft, methodology, visualization, writing – review and editing, data curation. **Zunli Lu:** funding acquisition, conceptualization, writing – review and editing, project administration, supervision, resources.

Acknowledgments

We acknowledge Karin Limburg and Debra Driscoll at the State University of New York School of Environmental Science and Forestry for their help with instrumentation. Tony Wang provided the coral sample. This work was supported by the Geological Society of America William B. & Dorothy Heroy Research Grant to A.N.P. and the NSF EAR 2121445 to Z.L.

Data Availability Statement

The data that support the findings of this study are available from the corresponding author upon reasonable request.

Peer Review

The peer review history for this article is available at https://www.webofscience.com/api/gateway/wos/peer-review/10.1002/rcm.10002.

References

1. Y. Kawakubo, Y. Yokoyama, A. Suzuki, et al., "Precise Determination of Sr/Ca by Laser Ablation ICP-MS Compared to ICP-AES and Application to Multi-Century Temperate Corals," *Geochemical Journal* 48, no. 2 (2014): 145–152, https://doi.org/10.2343/geochemj.2.0295.

2. J. Raddatz, A. Rüggeberg, S. Flögel, et al., "The Influence of Seawater pH on U/Ca Ratios in the Scleractinian Cold-Water Coral," *Biogeosciences* 11, no. 7 (2014): 1863–1871, https://doi.org/10.5194/bg-11-1863-2014.

3. T. Ourbak, T. Corrège, B. Malaizé, F. Le Cornec, K. Charlier, and J. P. Peypouquet, "A High-Resolution Investigation of Temperature, Salinity, and Upwelling Activity Proxies in Corals," *Geochemistry, Geophysics, Geosystems* 7, no. 3 (2006): 2005GC001064, https://doi.org/10.1029/2005GC001064.

4. Y. J. Sun, L. F. Robinson, I. J. Parkinson, et al., "Iodine-to-Calcium Ratios in Deep-Sea Scleractinian and Bamboo Corals," *Frontiers in Marine Science* 10 (2023): 1264380, https://doi.org/10.3389/fmars.2023.1264380.

5. W. Lu, C. F. Barbosa, A. E. Rathburn, et al., "Proxies for Paleo-Oxygenation: A Downcore Comparison Between Benthic Foraminiferal Surface Porosity and I/Ca," *Palaeogeography, Palaeoclimatology, Palaeoecology* 579, no. July (2021): 110588, https://doi.org/10.1016/j.palaeo.2021.110588.

6. J. Y. Chai and Y. Muramatsu, "Determination of Bromine and Iodine in Twenty-Three Geochemical Reference Materials by ICP-MS," *Geostandards and Geoanalytical Research* 31, no. 2 (2007): 143–150, https://doi.org/10.1111/j.1751-908X.2007.00856.x.

7. B. Williams and A. G. Grottoli, "Solution and Laser Ablation Inductively Coupled Plasma–Mass Spectrometry Measurements of Br, I, Pb, Mn, Cd, Zn, and B in the Organic Skeleton of Soft Corals and Black Corals," *Geochemistry, Geophysics, Geosystems* 12, no. 3 (2011): 2010GC003375, https://doi.org/10.1029/2010GC003375.

8. N. G. Prouty, E. B. Roark, L. M. Mohon, and C. C. Chang, "Uptake and Distribution of Organo-Iodine in Deep-Sea Corals," *Journal of Environmental Radioactivity* 187 (2018): 122–132, https://doi.org/10.1016/j.jenvrad.2018.01.003.

9. S. A. Wilson, A. E. Koenig, and R. Orklid, "Development of Microanalytical Reference Material (MACS-3) for LA-ICP-MS Analysis of Carbonate Samples," *Geochimica et Cosmochimica Acta* 72, no. 12 (2008): A1025.

10. K. E. Limburg, B. D. Walther, Z. Lu, et al., "In Search of the Dead Zone: Use of Otoliths for Tracking Fish Exposure to Hypoxia," *Journal of Marine Systems* 141 (2015): 167–178, https://doi.org/10.1016/j.jmarsys.2014.02.014.

11. R. He, K. E. Limburg, B. D. Walther, M. A. Samson, and Z. Lu, "Iodine Content of Fish Otoliths in Species Found in Diverse Habitats," *Environmental Biology of Fishes* 105 (2022): 351–367, https://doi.org/10.1007/s10641-022-01228-6.

12. E. C. Hathorne, R. H. James, P. Savage, and O. Alard, "Physical and Chemical Characteristics of Particles Produced by Laser Ablation of Biogenic Calcium Carbonate," *Journal of Analytical Atomic Spectrometry* 23, no. 2 (2008): 240–243, https://doi.org/10.1039/b706727e.

13. E. C. Hathorne, T. Felis, R. H. James, and A. Thomas, "Laser Ablation ICP-MS Screening of Corals for Diagenetically Affected Areas Applied to Tahiti Corals From the Last Deglaciation," *Geochimica et Cosmochimica Acta* 75, no. 6 (2011): 1490–1506, https://doi.org/10.1016/j.gca.2010.12.011.

14. W. Boer, S. Nordstad, M. Weber, et al., "New Calcium Carbonate Nano-Particulate Pressed Powder Pellet (NFHS-2-NP) for LA-ICP-OES, LA-(MC)-ICP-MS and μXRF," *Geostandards and Geoanalytical Research* 46, no. 3 (2022): 411–432, https://doi.org/10.1111/ggr.12425.

15. Origin (Pro),Version, *OriginLab Corporation* (MA, USA: Northampton, 2024).

16. H. P. Longerich, S. E. Jackson, and D. Günther, "Laser Ablation Inductively Coupled Plasma Mass Spectrometric Transient Signal Data Acquisition and Analyte Concentration Calculation," *Journal of Analytical Atomic Spectrometry* 11, no. 9 (1996): 899–904, https://doi.org/10.1039/JA9961100899.

17. D. J. Sinclair, L. P. J. Kinsley, and M. T. McCulloch, "High Resolution Analysis of Trace Elements in Corals by Laser Ablation ICP-MS," *Geochimica et Cosmochimica Acta* 62, no. 11 (1998): 1889–1901, https://doi.org/10.1016/S0016-7037(98)00112-4.

18. S. W. Smith, "Chapter 15: Moving Average Filters," in *The Scientist and Engineer's Guide to Digital Signal Processing*, 1st ed. (San Diego, CA: California Technical Publishing, 1997).

19. Gedcke DA. How Counting Statistics Controls Detection Limits and Peak Precision. accessed October 14, 2024, https://www.ortec-online.com/-/media/ametekortec/application-notes/an59.pdf?la=en&revision=882b9886-9534-4c10-8e6f-b00c9703ed1e&hash=604254C7CC458EC9B2CE0E90ED4FD2DC#:~:text=Detection%20limits%20for%20a%20peak,the%2095%25%2Dconfidence%20limit.

20. A. Limbeck, P. Galler, M. Bonta, G. Bauer, W. Nischkauer, and F. Vanhaecke, "Recent Advances in Quantitative LA-ICP-MS Analysis: Challenges and Solutions in the Life Sciences and Environmental Chemistry ABC Highlights: Authored by Rising Stars and Top Experts," *Analytical and Bioanalytical Chemistry* 407, no. 22 (2015): 6593–6617, https://doi.org/10.1007/s00216-015-8858-0.

21. K. P. Jochum, U. Nohl, K. Herwig, E. Lammel, B. Stoll, and A. W. Hofmann, "GeoReM: A New Geochemical Database for Reference Materials and Isotopic Standards," *Geostandards and Geoanalytical*

Research 29, no. 3 (2005): 333–338, https://doi.org/10.1111/j.1751-908X.2005.tb00904.x.

22. Z. Lu, H. C. Jenkyns, and R. E. M. Rickaby, "Iodine to Calcium Ratios in Marine Carbonate as a Paleo-Redox Proxy During Oceanic Anoxic Events," *Geology* 38, no. 12 (2010): 1107–1110, https://doi.org/10.1130/G31145.1.

23. J. T. Caulfield, E. L. Tomlinson, D. M. Chew, et al., "Microanalysis of Cl, Br and I in Apatite, Scapolite and Silicate Glass by LA-ICP-MS," *Chemical Geology* 557, no. July (2020): 119854, https://doi.org/10.1016/j.chemgeo.2020.119854.

24. M. A. Kendrick, J. T. Caulfield, A. D. Nguyen, J. Zhao, and I. Blakey "Halogen and Trace Element Analysis of Carbonate-Veins and Fe-Oxyhydroxide by LA-ICPMS: Implications for Seafloor Alteration, Atlantis Bank, SW Indian Ridge," *Chemical Geology* 547, no. May (2020): 119668, https://doi.org/10.1016/j.chemgeo.2020.119668.

25. G. Yang, H. Tazoe, and M. Yamada, "Improved Approach for Routine Monitoring of 129I Activity and 129I/127I Atom Ratio in Environmental Samples Using TMAH Extraction and ICP-MS/MS," *Analytica Chimica Acta* 1008 (2018): 66–73, https://doi.org/10.1016/j.aca.2017.12.049.

26. Kutscher D, Wills J, Ducos SM. Application Brief 43260 Interference Free Detection of the Radioactive Iodine Isotope 129-I Using Oxygen as a Reactive Gas. Published Online 2016. accessed October 18, 2024, https://tools.thermofisher.com/content/sfs/brochures/AB-43260-Iodine-Isotope-129I-Oxygen-AB43260-EN-HR.pdf.

27. A. V. Lazartigues, P. Sirois, and D. Savard, "LA-ICP-MS Analysis of Small Samples: Carbonate Reference Materials and Larval Fish Otoliths," *Geostandards and Geoanalytical Research* 38, no. 2 (2014): 225–240, https://doi.org/10.1111/j.1751-908X.2013.00248.x.

28. K. P. Jochum, B. Stoll, U. Weis, D. E. Jacob, R. Mertz-Kraus, and M. O. Andreae, "Non-Matrix-Matched Calibration for the Multi-Element Analysis of Geological and Environmental Samples Using 200 nm Femtosecond LA-ICP-MS: A Comparison With Nanosecond Lasers," *Geostandards and Geoanalytical Research* 38, no. 3 (2014): 265–292, https://doi.org/10.1111/j.1751-908X.2014.12028.x.

29. D. Garbe-Schönberg and S. Müller, "Nano-Particulate Pressed Powder Tablets for LA-ICP-MS," *Journal of Analytical Atomic Spectrometry* 29, no. 6 (2014): 990–1000, https://doi.org/10.1039/C4JA00007B.

30. R. Machida, T. Nakazawa, and N. Furuta, "Temporal Changes of Fractionation Index Caused by Changes in the Large Size of Ablated Particles in Laser Ablation-Inductively Coupled Plasma Mass Spectrometry," *Analytical Sciences* 31, no. 5 (2015): 345–355, https://doi.org/10.2116/analsci.31.345.

31. J. D. Woodhead, J. Hellstrom, J. M. Hergt, A. Greig, and R. Maas, "Isotopic and Elemental Imaging of Geological Materials by Laser Ablation Inductively Coupled Plasma-Mass Spectrometry," *Geostandards and Geoanalytical Research* 31, no. 4 (2007): 331–343, https://doi.org/10.1111/j.1751-908X.2007.00104.x.

32. W. T. Perkins, R. Fuge, and N. J. G. Pearce, "Quantitative Analysis of Trace Elements in Carbonates Using Laser Ablation Inductively Coupled Plasma Mass Spectrometry," *Journal of Analytical Atomic Spectrometry* 6, no. 6 (1991): 445, https://doi.org/10.1039/ja9910600445.

33. J. S. Fehrenbacher, H. J. Spero, A. D. Russell, L. Vetter, and S. Eggins, "Optimizing LA-ICP-MS Analytical Procedures for Elemental Depth Profiling of Foraminifera Shells," *Chemical Geology* 407–408 (2015): 2–9, https://doi.org/10.1016/j.chemgeo.2015.04.007.

34. Y. G. Yingling and B. J. Garrison, "Photochemical Induced Effects in Material Ejection in Laser Ablation," *Chemical Physics Letters* 364, no. 3–4 (2002): 237–243, https://doi.org/10.1016/S0009-2614(02)01327-1.

35. V. Warter and W. Müller, "Daily Growth and Tidal Rhythms in Miocene and Modern Giant Clams Revealed via Ultra-High Resolution LA-ICPMS Analysis—A Novel Methodological Approach Towards Improved Sclerochemistry," *Palaeogeography, Palaeoclimatology, Palaeoecology* 465 (2017): 362–375, https://doi.org/10.1016/j.palaeo.2016.03.019.

36. A. Cohen, S. Smith, M. McCartney, and J. Van Etten, "How Brain Corals Record Climate: An Integration of Skeletal Structure, Growth and Chemistry of Diploria Labyrinthiformis From Bermuda," *Marine Ecology Progress Series* 271 (2004): 147–158, https://doi.org/10.3354/meps271147.

37. sWever SO. "Diploria Labryinthiformis Close-Up".

38. A. J. Reichelt-Brushett and G. McOrist, "Trace Metals in the Living and Nonliving Components of Scleractinian Corals," *Marine Pollution Bulletin* 46, no. 12 (2003): 1573–1582, https://doi.org/10.1016/S0025-326X(03)00323-0.

39. A. C. Gagnon, J. F. Adkins, D. P. Fernandez, and L. F. Robinson, "Sr/ca and mg/ca Vital Effects Correlated With Skeletal Architecture in a Scleractinian Deep-Sea Coral and the Role of Rayleigh Fractionation," *Earth and Planetary Science Letters* 261, no. 1–2 (2007): 280–295, https://doi.org/10.1016/j.epsl.2007.07.013.

40. B. Kaczorowska, A. Hacura, T. Kupka, et al., "Spectroscopic Characterization of Natural Corals," *Analytical and Bioanalytical Chemistry* 377, no. 6 (2003): 1032–1037, https://doi.org/10.1007/s00216-003-2153-1.

Supporting Information

Additional supporting information can be found online in the Supporting Information section.